Fully developed turbulent flow of non-Newtonian liquids through a square duct

M P Escudier and S Smith

University of Liverpool
Department of Engineering, Mechanical Engineering

18 April 2000

Abstract

The results are reported of an experimental investigation of fully developed turbulent flow through an 80mm x 80mm duct of water and of two shear-thinning polymers, an aqueous solution of 0.1% carboxymethylcellulose + 0.1% xanthan gum (CMC/XG) and a 0.125% aqueous solution of polyacrylamide (PAA). The more elastic PAA leads to drag-reduction levels up to 77% compared with 65% for CMC/XG. It is well established (e.g. Nikuradse (1930), Melling and Whitelaw (1976) that contours of mean axial velocity are a good indicator of the strength of the turbulence-induced secondary flow. We find that for water the contours away from the walls and the channel centre bulge towards the corners as a consequence of the transport of fluid with high axial momentum into regions where the momentum would otherwise be low. For CMC/XG this tendency is much reduced and absent for PAA.

Over much of the duct cross section the contours of axial turbulence intensity $\tilde{u}_1/U_C$ for water and CMC/XG are similar to each other and to the contours for water reported by Melling and Whitelaw. In the vicinity of the duct centreline the levels for CMC/XG are slightly lower than for water and the peak $\tilde{u}_1$ values are about 0.15 U for both flows. For CMC/XG the peak values occur well away from the duct wall whereas for water the levels increase all the way to the wall. For PAA the peak $\tilde{u}_1/U_C$ values are reduced by about 50% and the tendency for the contours to push into the corners is suppressed.

Below the diagonal bisector (sector 2) the turbulence intensity $\tilde{u}_3$ corresponds to fluctuations parallel to the duct wall $(\tilde{w})$ and above the diagonal (sector 1) to fluctuations normal to the wall $(\tilde{v})$. For water the contours are again similar to those reported by Melling and Whitelaw. For all three fluids $\tilde{w} > \tilde{v}$ over most of the duct cross section. As for $\tilde{u}_1$, the peak values of $\tilde{v}$ and $\tilde{w}$ for CMC/XG and for PAA occur on the wall bisector some distance away from the duct wall whereas for water both peaks are closer to the wall. The overall turbulent kinetic energy levels are slightly reduced for CMC/XG and greatly so for PAA. The levels of anisotropy for CMC/XG and PAA are similar and much greater than for water.

For CMC/XG the $\overline{u_1u_3}$ values are only about 40% of those for water while the levels for PAA are barely distinguishable from the background noise. For water the maximum value of $\overline{u_1u_3}$ (in sector 2) is about 15% of that of $-\overline{u_1u_3}$ (in sector 1) whereas for CMC/XG the ratio is closer to 0.5 and for PAA the two are of the same magnitude.

1. Introduction

Previous investigations, by Kostic and Hartnett (1985), Hartnett et al (1986), Hartnett and Kostic (1990), Kostic (1994), and Hartnett and Rao (1987), have shown that, in terms of global hydrodynamic behaviour, fully developed flow of a non-Newtonian liquid through a square duct is little different from turbulent flow of the same fluid through a circular tube. For the flow of strongly viscoelastic (and shear-thinning) liquids, measured frictional pressure-drop data for a square duct were found by Hartnett et al (1986) to be in excellent agreement with Cho and Hartnett's (1982) correlation

$$f = 0.2\,\mathrm{Re}^{-0.48} \tag{1}$$

where the Fanning friction factor is defined as

$$f \equiv \frac{\tau_s}{\rho U^2} \tag{2}$$

τ_s being the average wall shear stress, ρ the fluid density and U the bulk mean velocity and Re is the Reynolds number based upon the hydraulic diameter D_H and the apparent viscosity at the duct wall. In fact, the data of Hartnett et al (1986) also correlate extremely well with a "generalised" version of equation (1)

i.e.
$$f = 0.2\,\mathrm{Re}^{*\,-0.48}. \tag{3}$$

where Re^* is the generalised Reynolds number for a power-law fluid defined by Kozicki et al (1966) as

$$\mathrm{Re}^* \equiv \frac{\rho U^{2-n} D_H^n}{8^{n-1} K\left(b + \frac{a}{n}\right)^n} \tag{4}$$

For a square duct Kozicki and Tiu (1971) give the values of the constants a and b as 0.1561 and 0.7326.

Although the foregoing suggests a satisfactory situation from an engineering viewpoint, for non-Newtonian fluids little is known of the underlying mean flow and turbulence structure. For a Newtonian fluid Nikuradse (1930) used a visualisation technique for flow through a rectangular duct to show the existence of secondary flows of Prandtl's (1952) second kind i.e. driven by gradients in the turbulent normal stresses. Melling and Whitelaw (1976) carried out extensive LDA measurements to quantify both this secondary motion and also the turbulence structure. After careful consideration of the available experimental data, Demuren and Rodi (1984) concluded from the equation for streamwise vorticity that the origin of the secondary motion is the second-order terms of the difference in the gradients of the Reynolds stresses

i.e.
$$\frac{\partial^2}{\partial x_2 \partial x_3}\left(\widetilde{u}_3^{\,2} - \widetilde{u}_2^{\,2}\right) - \left(\frac{\partial^2}{\partial x_3^2} - \frac{\partial^2}{\partial x_2^2}\right)\overline{u_2 u_3} \tag{5}$$

This conclusion was supported by the more recent numerical work of Wang et al (1994).

Rudd (1972) and Logan (1972) reported limited measurements of the mean flow and turbulence structure for flow of drag-reducing polymers through square tubes. For these experiments the polymer concentrations were sufficiently low (0.01% and 0.005%, respectively), that the fluid rheology was practically that of the solvent (water). Also, both investigators confined their measurements to a traverse along one wall bisector and so could provide no information about the secondary flow. More recently Gampert and Rensch (1996) have reported the results of a systematic study of the influence of polymer concentration on near-wall turbulence structure for the flow of polyacrylamide through a square duct but again provide no direct information on the secondary flow.

The partial suppression of transverse turbulence fluctuations is well established for the pipe-flow of drag-reducing liquids (see e.g. Escudier et al (1999)) and it has been speculated (Kostic (1994)) that the same will be the case for flow through a square duct. The recent paper of Warholic et al (1999) shows that the same behaviour occurs in fully-developed channel flow. It has to be expected therefore that the turbulence-induced secondary motion will also be largely suppressed and this in turn will create less bulging of the axial flow i.e. there will be reduced transport of fluid of high axial momentum into the corners of the duct. It is well known that secondary flows also arise in the fully developed laminar flow of viscoelastic liquids: the detailed

calculations of Wheeler and Wissler (1966) for flow through a square duct show that the normal force differences which arise along the boundary surface drive a secondary flow in a direction counter to that which arises due to turbulence in a Newtonian fluid.

In the present paper we present both global data (friction-factor versus Reynolds number) and detailed mean axial- and secondary-flow-velocity and turbulence-field data for fully developed flow through a square duct of two non-Newtonian liquids, both of which are shear thinning and viscoelastic. We also include data for a Newtonian fluid (water) as a basis for comparison.

2. Experimental rig and instrumentation

The flow loop used for the experiments, is a modified version of that used by Escudier et al (1999) for their pipe-flow investigation. The square duct consisted of ten stainless steel modules each of length 1.2 m and with a square internal cross section of side length D = 80 mm. One module 9.6 m from the inlet connection was assembled with borosilicate-glass sidewalls to permit measurements using a laser Doppler anemometer. Distributions of mean velocity and turbulence structure were obtained from LDA traverses along the horizontal lines in the upper right quadrant of the duct as shown in **Figure 1**. A flow straightener fabricated from aluminium-alloy honeycomb was installed at the inlet to the test section for the final series of experiments.

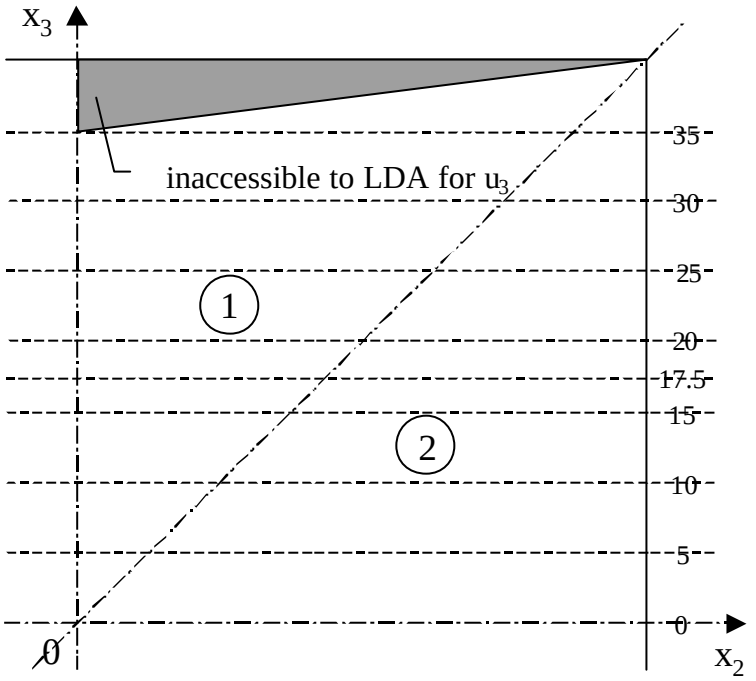

Figure 1. Coordinate system for duct-flow measurements

Measurements were made of the distributions of the mean velocity and turbulence structure 130 hydraulic diameters (10.4 m) downstream of the duct inlet using a Dantec Fibreflow laser Doppler anemometer system comprising a 60X10 probe and 55X12 beam expander together with two Dantec Burst Spectrum Analyzer signal processors (one model 57N10, the other model 57N20). The LDA optical parameters were as follows: beam separation at front lens 51.5 mm, lens focal length 160 mm, length of principal axis of measurement volume 0.21 mm and diameter 0.02 mm. All velocity measurements were biased according to residence time. In view of the small size of the measurement volume, it was not felt necessary to make any gradient correction to the measured velocities.

The shear viscosity and first normal-stress difference characteristics of the polymeric test fluids were determined using a Bohlin VOR controlled shear-rate rheometer with either a concentric cylinder (double gap), a cone-and-plate or a parallel-plate geometry.

3. Working fluid characteristics

Measurements were made with water, as a Newtonian control fluid; with an aqueous solution of 0.1% w/w high viscosity grade sodium carboxymethylcellulose (CMC), supplied by Aldrich Chemical Company, blended with 0.1% w/w xanthan gum (XG), a food grade supplied by the Kelco Division of Merck and Co Inc; and with an

aqueous solution of 0.125% w/w polyacrylamide (PAA), Separan AP273 supplied by Floerger. The viscosity curves for the two polymer solutions are well represented by the Cross model for a shear-thinning liquid

$$\frac{\mu_0 - \mu}{\mu_0 - \mu_\infty} = (\lambda\dot{\gamma})^m . \qquad (6)$$

The values for the four parameters in the Cross equation of the two working liquids are listed in **Table 1** and the corresponding experimental data are plotted in **Figure 2** together with viscosity curves representing the Cross-model fits.

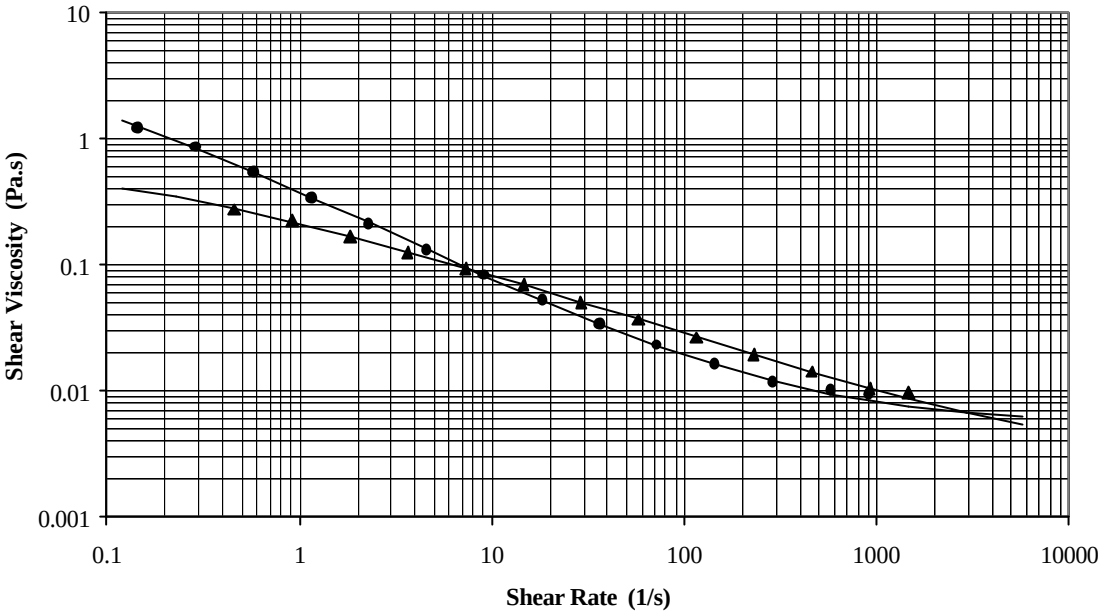

Figure 2. Viscosity curves for ▲ 0.1% CMC/0.1% XG and ● 0.125% PAA together with Cross-model fits.

Table 1 Cross-model and power-law parameters

	CMC/XG (19^oC)	PAA (20^oC)
μ_0 (Pa.s)	0.681	5.25
μ_∞ (Pa.s)	0.00328	0.00558
λ (s)	3.21	34.3
m	0.552	0.733
K(Pa.s^n)	0.275	0.373
n	0.519	0.313

At the concentrations used for the flow experiments, the first normal stress differences for CMC/XG were below the sensitivity of the rheometer even at the highest shear rates. However, as suggested by Barnes et al (1989), at higher concentrations it was found that $N_1(\tau)$ followed a power-law master curve for each fluid, practically independent of concentration, from which it was possible to extrapolate to lower concentrations. The data result in the empirical expression

$$N_1 = 1.35\tau^{1.18} \qquad 0.8/0.8\text{-}1.5/1.5\%\ \text{CMC/XG} \qquad (7)$$

According to Barnes et al, a recoverable shear (i.e. $N_1/2\tau$) greater than 0.5 indicates a highly elastic state, a condition for CMC/XG which corresponds to shear stresses in excess of 0.2 Pa. For PAA it was possible to obtain $N_1(\dot{\gamma})$ data directly because even at a concentration as low as 0.125% the N_1 values were significantly above the resolution of the rheometer. The data are well represented by

$$N_1 = 16.3\ \tau^{1.48} \qquad 0.125\%\ \text{PAA} \qquad (8)$$

so that 0.125% PAA can be said to be highly elastic for $\tau > 0.003$.

4. Friction factors and transition

Fanning friction factors calculated from the measured pressure gradient are plotted versus the generalised Reynolds number Re^* in **Figure 3**. For values of Re^* below about 2000 the friction-factor data are well correlated as expected by

$$f = \frac{16}{Re^*}. \qquad (9)$$

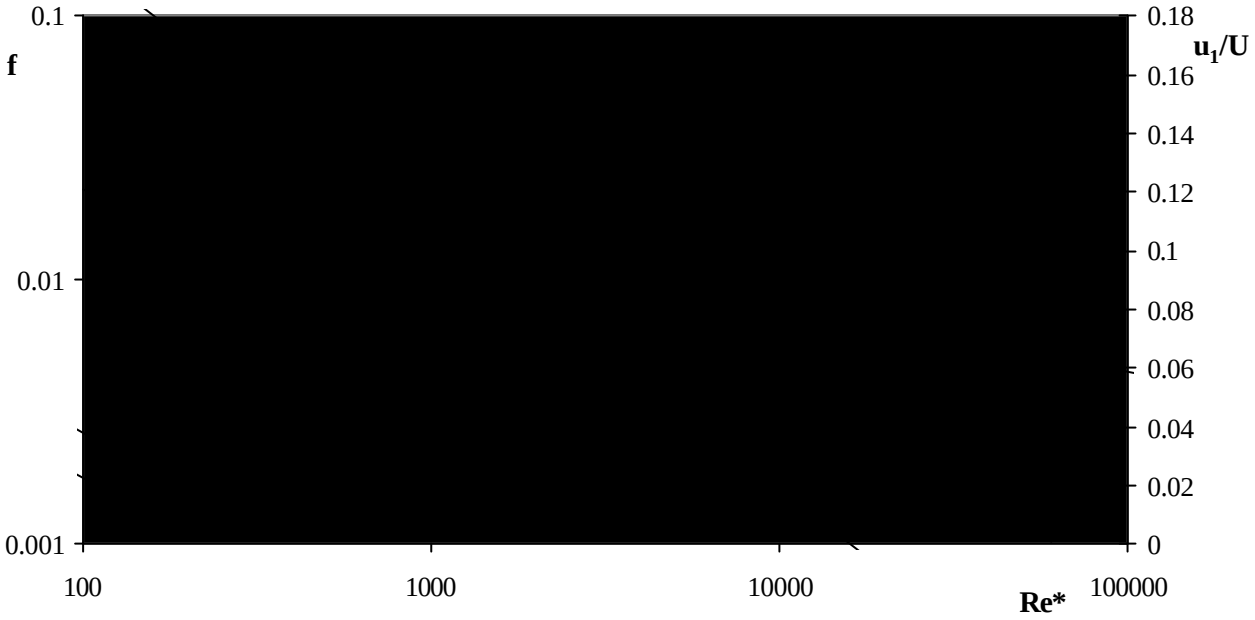

Figure 3. Fanning friction factor (closed symbols) and near-wall turbulence intensity (open symbols) versus generalised Reynolds number: ■ water, ◆ ? CMC/XG, ● ○ PAA.

For higher Re^* values the flows are turbulent and the data for the two polymers approach the pipe-flow correlation of Cho and Hartnett (1982) with Re replaced by Re^* (equation (3)), and indicate drag-reduction levels up to 65% for CMC/XG (at $Re^* = 10{,}500$) and 77% for PAA ($Re^* = 21{,}400$). The drag-reduction levels were calculated with respect to the Blasius equation for a Newtonian fluid

$$f = 0.0791\ Re^{*-0.25}. \qquad (10)$$

Values for the rms axial turbulence intensity $\tilde{u}_1$ measured 10 mm from the duct wall on one of the wall bisectors indicate an increase above background levels at $Re^* \approx 1000$ with a rapid increase from $Re^* \approx 3000$ to peaks in the region of $Re^* = 7000$ beyond which the $\tilde{u}_1$ levels begin to fall. This increase in $\tilde{u}_1$ has been shown by Park et al (1989) and others to be a good indicator of transition in pipe flow and we conclude from the data in **Figure 3** that for duct flow of the two polymers the flow is fully turbulent for $Re^* > 7000$. Detailed measurements of the mean flow and turbulence field were made at flowrates close to the highest achievable, corresponding to Re^* values of 10,500 for CMC/XG and 16,400 for PAA. The water-flow experiments were carried out for $Re^* = 43{,}000$ which is close to that for the investigation of Melling and Whitelaw (1976). Values for Re*, Re and other global flow parameters are listed in **Table 2**.

Table 2 Global flow parameters

	H_2O	CMC/XG	PAA
U (m/s)	0.478	2.54	2.17
$10^3 f$	5.06	2.80	1.84
u_τ (m/s)	0.024	0.095	0.066
$10^{-4} Re$	4.29	2.08	1.76
$10^{-4} Re^*$	4.83	1.05	1.64

5. Mean flow and turbulence structure

5.1. Mean primary-flow axial velocity $\overline{u}_1$

It is well established (e.g. Nikuradse (1930), Melling and Whitelaw (1976)) that contours of mean axial velocity as shown in **Figure 4** are a good indicator of the strength of the turbulence-induced secondary flow. For water (**Figure 4 (a)**) there is a tendency for the contours away from the walls and the channel centre to bulge towards the corners as a consequence of the transport of fluid with high axial momentum into regions where the momentum would otherwise be low. For CMC/XG (**Figure 4 (b)**) this tendency is much reduced and completely absent for PAA (**Figure 4 (c)**). The combined influence of the change in profile shape associated with drag reduction and the reduced secondary flow is apparent in the ratios U_C/U listed in **Table 3**.

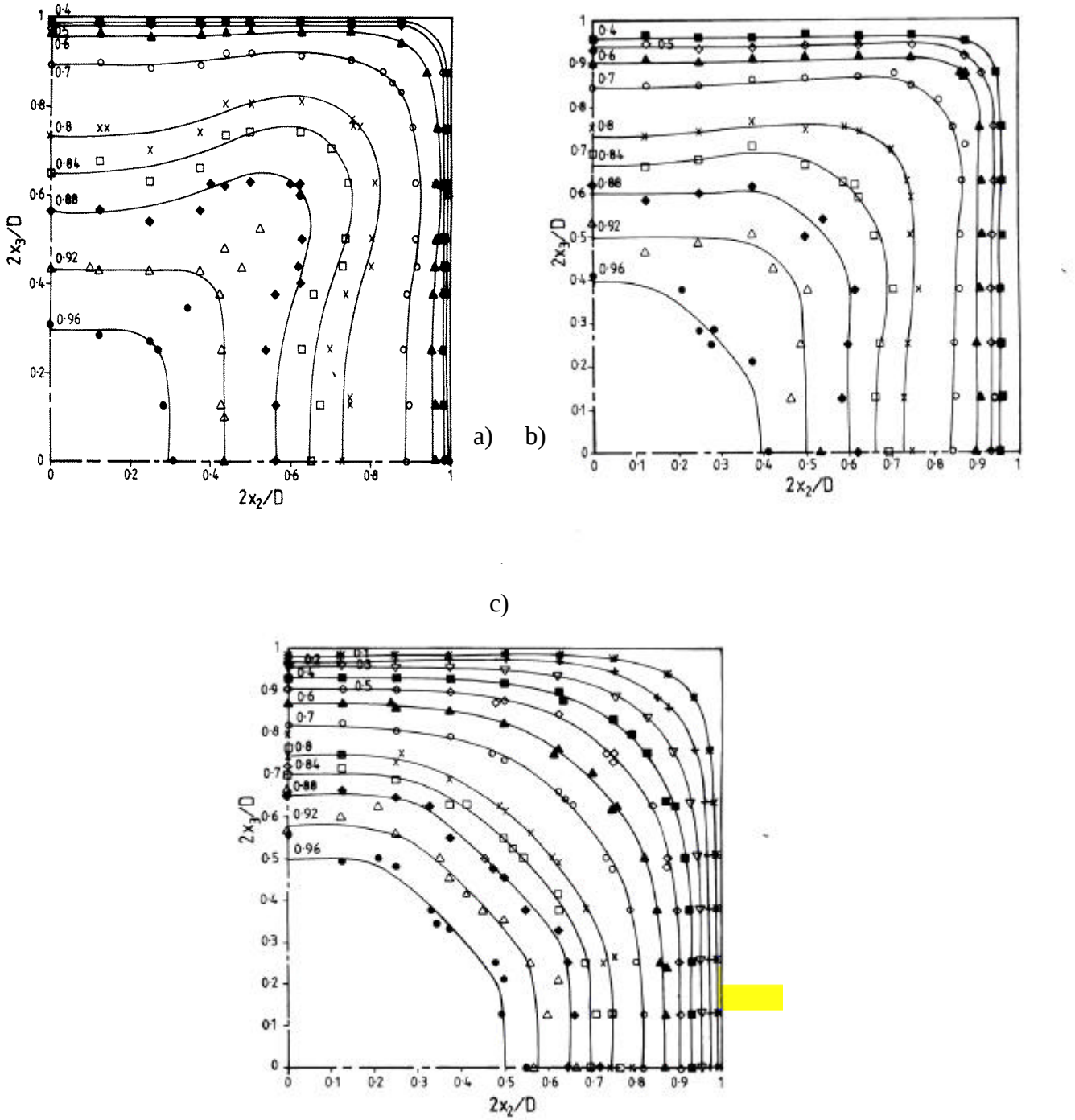

Figure 4. Mean flow axial-velocity isovels $\overline{u}_1/U_C$ (a) water (b) CMC/XG (c) PAA.

Table 3 Peak values of mean-flow and turbulence quantities

	H_2O	CMC/XG	PAA
U_C/U	1.22	1.29	1.41
$\overline{u}_3/U$	0.0281	0.0063	0.0045
$\tilde{u}_1/U$	0.148	0.156	0.084
$\tilde{u}_1^+$	2.91	4.20	2.77
$\tilde{v}/U$	0.057	0.030	0.016
$\tilde{v}^+$	1.12	0.80	0.54
$\tilde{w}/U$	0.077	0.043	0.028
$\tilde{w}^+$	1.51	1.16	0.92
$\overline{u_1 u_3}/U^2$	0.0022	0.0009	0.0002
$\overline{u_1^+ u_3^+}$	0.87	0.64	0.22

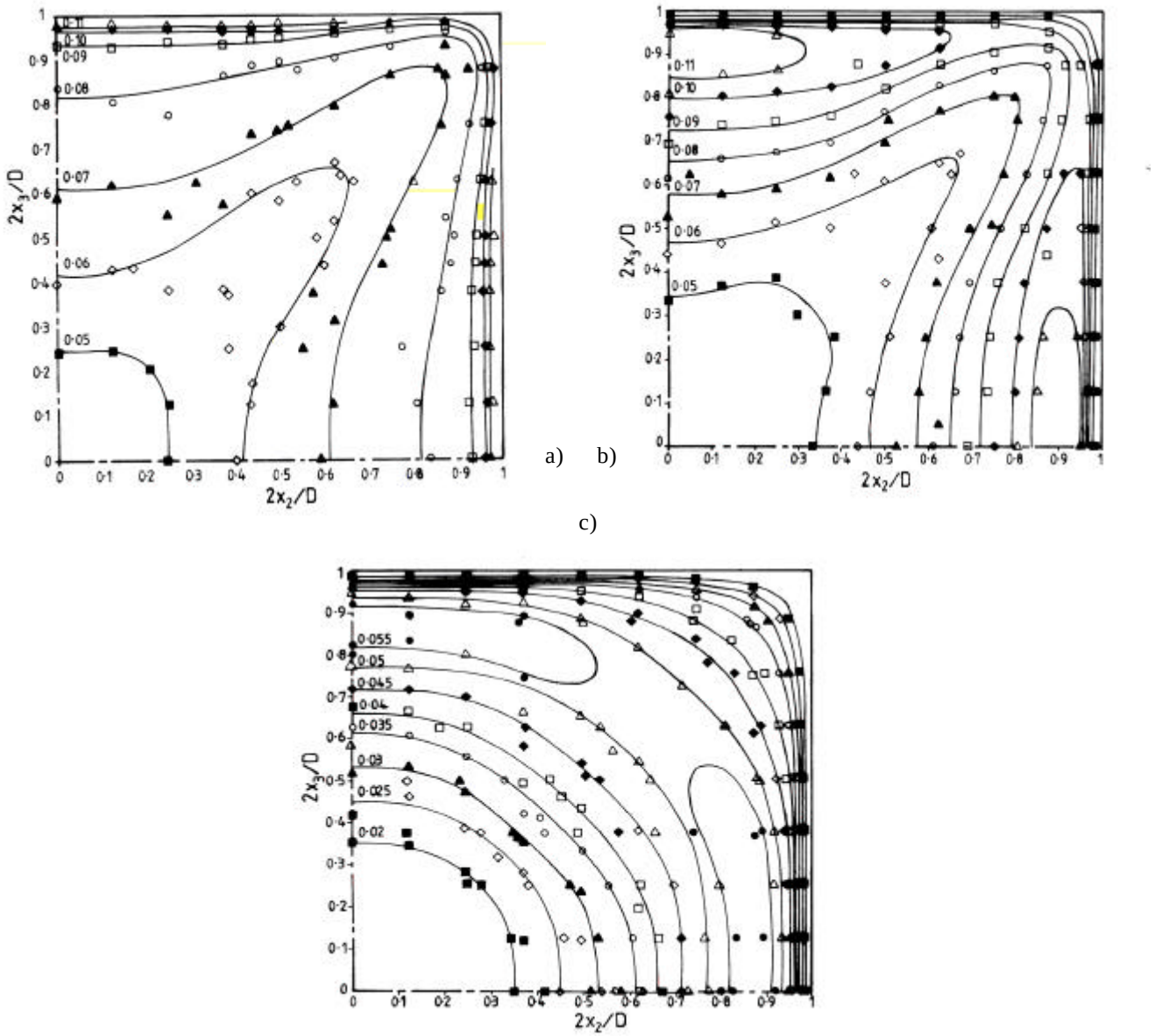

Figure 5. Contours of rms axial turbulence intensity $\tilde{u}_1/U_C$ (a) water (b) CMC/XG (c) PAA.

5.2 Rms axial turbulence intensity $\tilde{u}_1$

Over much of the duct cross section the contours of the normalised rms axial turbulence intensity $\tilde{u}_1/U_C$ for water and CMC/XG shown in **Figure 5** are clearly very similar to each other and to the contours for water flow reported by Melling and Whitelaw (1976). In the vicinity of the duct centreline the levels for CMC/XG are slightly lower than for water and the peak values are between 0.15 U and 0.16 U for both flows. A significant difference is that for CMC/XG the peak values given in **Table 3** occur well away from the duct wall (on the wall bisectors at $2x_2/D = 2x_3/D \approx 0.9$) whereas for water the levels increase all the way to the wall (within the region of measurement). Similar behaviour was observed by Presti (1998) for pipe flow of CMC/XG at a comparable Reynolds number but with increasing Reynolds number Presti found that the peak moved towards the pipe wall. For PAA (**Figure 5(c)**) the peak $\tilde{u}_1/U_C$ values have been reduced by about 50%, also much the same as found by Presti for pipe flow of PAA, and the tendency for the contours to push into the corners has been suppressed.

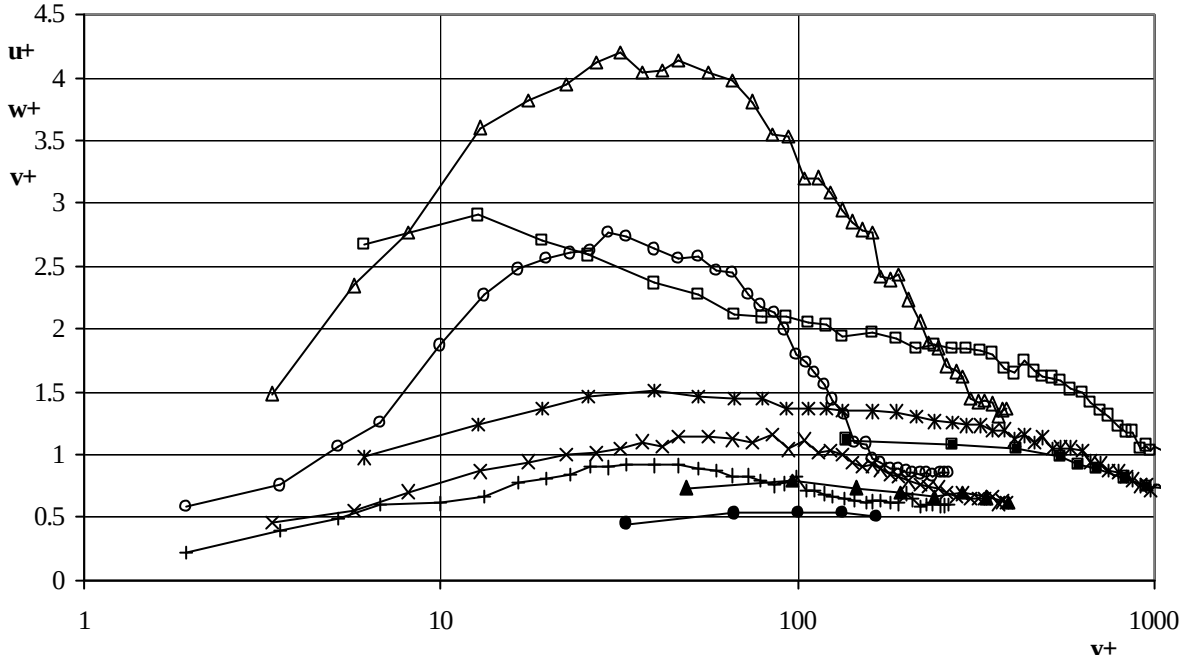

Figure 6. Rms turbulence intensities measured along the wall bisector in wall coordinates $\tilde{u}_1^+$, $\tilde{v}^+$ and $\tilde{w}^+$ versus y^+: □ ✻ ■ water, D ✕ ▲ CMC/XG, ○ + ● PAA

The streamwise turbulence-intensity data in wall coordinates measured along the mid-wall bisector (**Figure 6**) follow similar trends with increasing drag reduction to those reported by Gampert and Rensch (1996) and Warholic et al (1999). For water we find the peak value for $\tilde{u}_1^+$ is slightly less than 3 and located in the region $10 < y^+ < 20$. The peak for the CMC/XG data (drag reduction ca 65%) is much higher (~4.2) and shifted to higher y^+ (~40) whereas for PAA (drag reduction ca 74% at $Re^* = 16{,}400$) the magnitude of the $\tilde{u}_1^+$ peak is marginally smaller than that for water but again shifted to $y^+ \approx 40$. A convenient summary of our own $\tilde{u}_1^+$ data and that of Gampert and Rensch is provided by a plot (**Figure 7**) of the peak values ($\tilde{u}_{1,\,MAX}^+$) versus the degree of drag reduction at a given generalised Reynolds number expressed as a fraction of the maximum possible drag reduction calculated for the same value of the generalised Reynolds number

i.e. versus
$$\frac{f_{\text{Blasius}} - f_{\text{measured}}}{f_{\text{Blasius}} - f_{\text{Cho-Hartnett}}} \qquad (11)$$

where f_{Blasius} is calculated from equation (10) and $f_{\text{Cho-Hartnett}}$ from equation (3).

The data show an initial gradual increase in $\tilde{u}_{1,\,MAX}^+$ with increasing drag reduction followed by a very large and sudden decrease in $\tilde{u}_{1,\,MAX}^+$ for drag reduction close to the maximum possible. It should be noted that Gampert and Rensch's data correspond to increasing concentrations of the same polymer for two flowrates whereas our data relate to two different polymers and flowrates. It is unclear whether the tendency for drag reduction to increase and then decrease with increasing polymer concentration, as found by Gampert and Rensch, is real and associated with mixing, as found by Warholic et al, or is the result of experimental uncertainty.

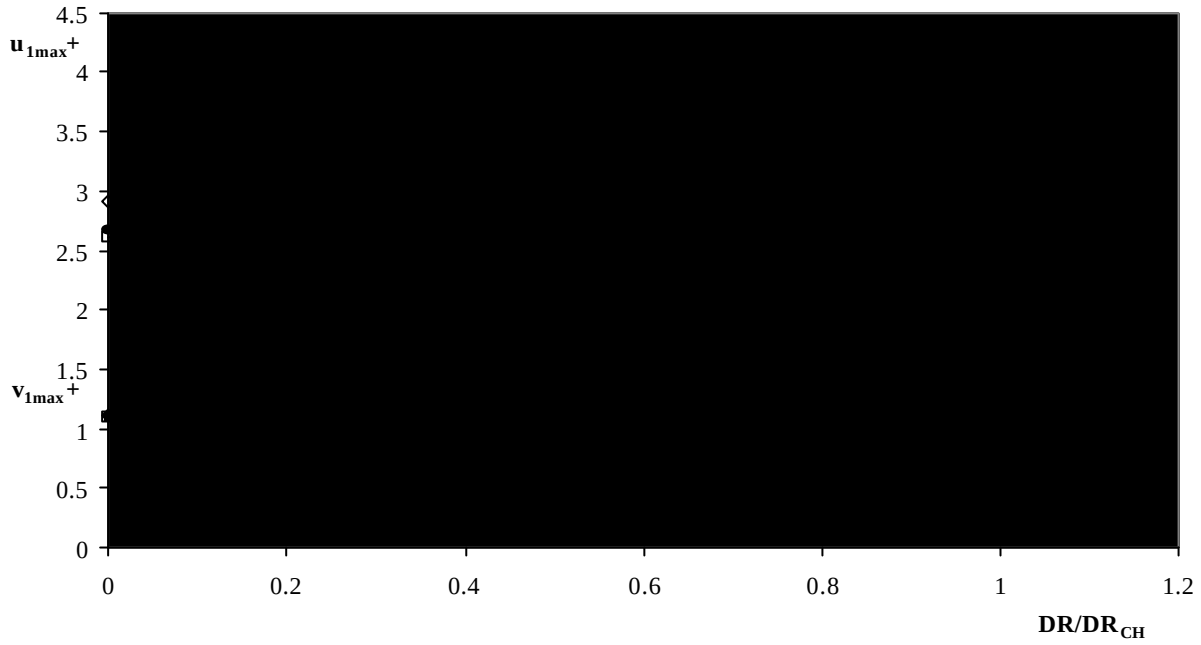

Figure 7 Peak rms turbulence intensities versus fractional drag reduction: $\tilde{u}_{1,MAX}^+$ ● □ Gampert and Rensch (1996), ? present data; $\tilde{v}_{MAX}^+$ ■ Gampert and Rensch, ◆ present data.

5.3 Transverse rms turbulence intensity $\tilde{u}_3$

In considering the transverse turbulence-intensity contours shown in **Figure 8**, it should be borne in mind that below the diagonal bisector (see **Figure 1**) the measured rms turbulence intensity $\tilde{u}_3$ corresponds to fluctuations parallel to the duct wall $(\tilde{w})$ and above the diagonal to fluctuations normal to the wall $(\tilde{v})$ i.e. the contours are asymmetric with respect to the diagonal although symmetry with respect to the wall bisectors is maintained. For water (**Figure 8 (a)**) the contours are again very similar to those reported by Melling and Whitelaw (1976) although we have constructed a contour from the measurements for $\tilde{w}/U_c = 0.04$ similar in appearance to that for $\tilde{w}/U_c = 0.045$ whereas the corresponding contour of Melling and Whitelaw is similar to that for $\tilde{w}/U_c = 0.035$. For all three fluids it is seen that over most of the duct cross section $\tilde{w} > \tilde{v}$. As for $\tilde{u}_1$, the peak values of both $\tilde{v}$ and $\tilde{w}$ for both CMC/XG (**Figure 8 (b)**) and for PAA (**Figure 8 (c)**) occur on the wall bisector some distance away from the duct wall whereas for water both peaks are closer to the wall. From **Table 3** it is seen that the peak values of $\tilde{w}$ for CMC/XG are about 56% of those for water (0.043 U compared with 0.077 U) while for PAA the values are only 36% (0.028 U) with the lower $\tilde{v}$ values following a similar pattern (0.057 U, 0.030 U, 0.016 U). The turbulence data also lead to the conclusion that the overall turbulent kinetic energy levels are slightly reduced for CMC/XG and greatly so for PAA. The level of anisotropy for CMC/XG and PAA is similar and much greater than for the water flow. Unfortunately over most of sector 1 (i.e. above the diagonal) the $\tilde{v}$ levels for PAA were generally too low for accurate measurements to be made.

The trends in our normal turbulence-intensity data in wall coordinates (**Figures 6** and **7**) are consistent with most previous pipe- and channel-flow data, including that reported in the recent study of Warholic et al (1999), but not with that of Gampert and Rensch. Almost all previous investigators have found that with increasing drag reduction $\tilde{v}$ decreases even more than u_τ so that $\tilde{v}_{MAX}^+$ decreases, as shown by our admittedly limited data in **Figure 7** whereas the data of Gampert and Rensch show little change in $\tilde{v}^+$ with increasing drag reduction However, Warholic et al question the reliability of Gampert and Rensch's $\tilde{v}$ measurements and state that they appear to be too large, which is consistent with **Figure 7**. The data in **Figure 6** show another trend which is consistent with Gampert and Rensch's findings: the peak values for both $\tilde{v}^+$ and $\tilde{w}^+$ for all three fluids occur at much larger values of y^+ than was the case for $\tilde{u}_1^+$. For $\tilde{w}^+$ the peaks occur at about $y^+ = 30$ for water and PAA and at about $y^+ = 55$ for CMC/XG. As a consequence of the limited optical access in Sector 1 there is little data for $\tilde{v}^+$ in the near-wall region, but the indications are that the peaks all occur at about $y^+ = 100$. It is only the peak in $\tilde{u}_1^+$, therefore, which

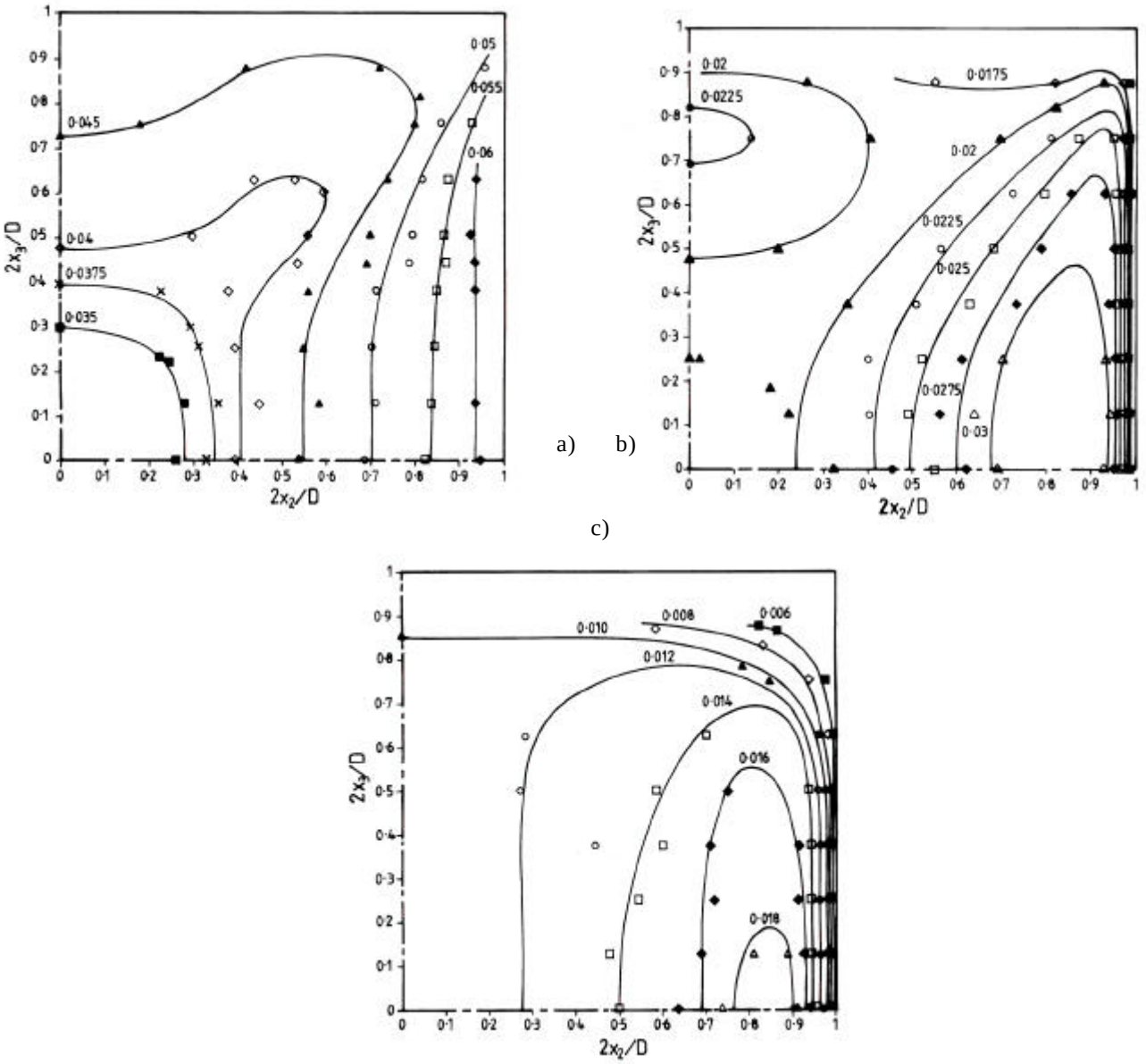

Figure 8. Contours of rms transverse turbulence intensity $\tilde{u}_3/U_C$ (a) water (b) CMC/XG (c) PAA.

shifts to higher y^+ values as a consequence of drag reduction. However, the reduction in the levels of $\tilde{v}^+$ increases with the degree of drag reduction, as found by Warholic et al and to a limited extent by Gampert and Rensch. The data in **Figure 6** show that the level of $\tilde{w}^+$ is reduced to much the same degree as $\tilde{v}^+$.

5.4 Reynolds shear stress $\overline{u_1 u_3}$

Similar remarks to those made in the previous subsection concerning the interpretation of $\tilde{v}$ and $\tilde{w}$ apply to $\overline{u_1 u_3}$. For CMC/XG (**Figure 9 (b)**) the $\overline{u_1 u_3}$ values are only about 40% of those for water (**Figure 9 (a)**) and the levels for PAA were barely distinguishable from the background noise so that **Figure 9 (c)** is included merely to indicate the qualitative structure of $\overline{u_1 u_3}$ for this fluid. Here our observations are consistent with both Gampert and Rensch and those of Warholic et al (1999) who found near-zero levels of Reynolds shear stress for levels of drag reduction in excess of 60%. For the water flow the maximum value of $\overline{u_1 u_3}$ (in sector 2) is about 15% of that of $-\overline{u_1 u_3}$ (in sector 1) whereas for CMC/XG the ratio is closer to 0.5 and the limited data for PAA suggests that for this fluid the two are of roughly the same magnitude. Unfortunately, as already noted, the region close to the upper duct wall (see **Figure 1**) was inaccessible to the LDA and the form of the $\overline{u_1 u_3}$ contours in this region merely indicate the trends indicated by theoretical considerations (e.g. by Wang et al (1994)).

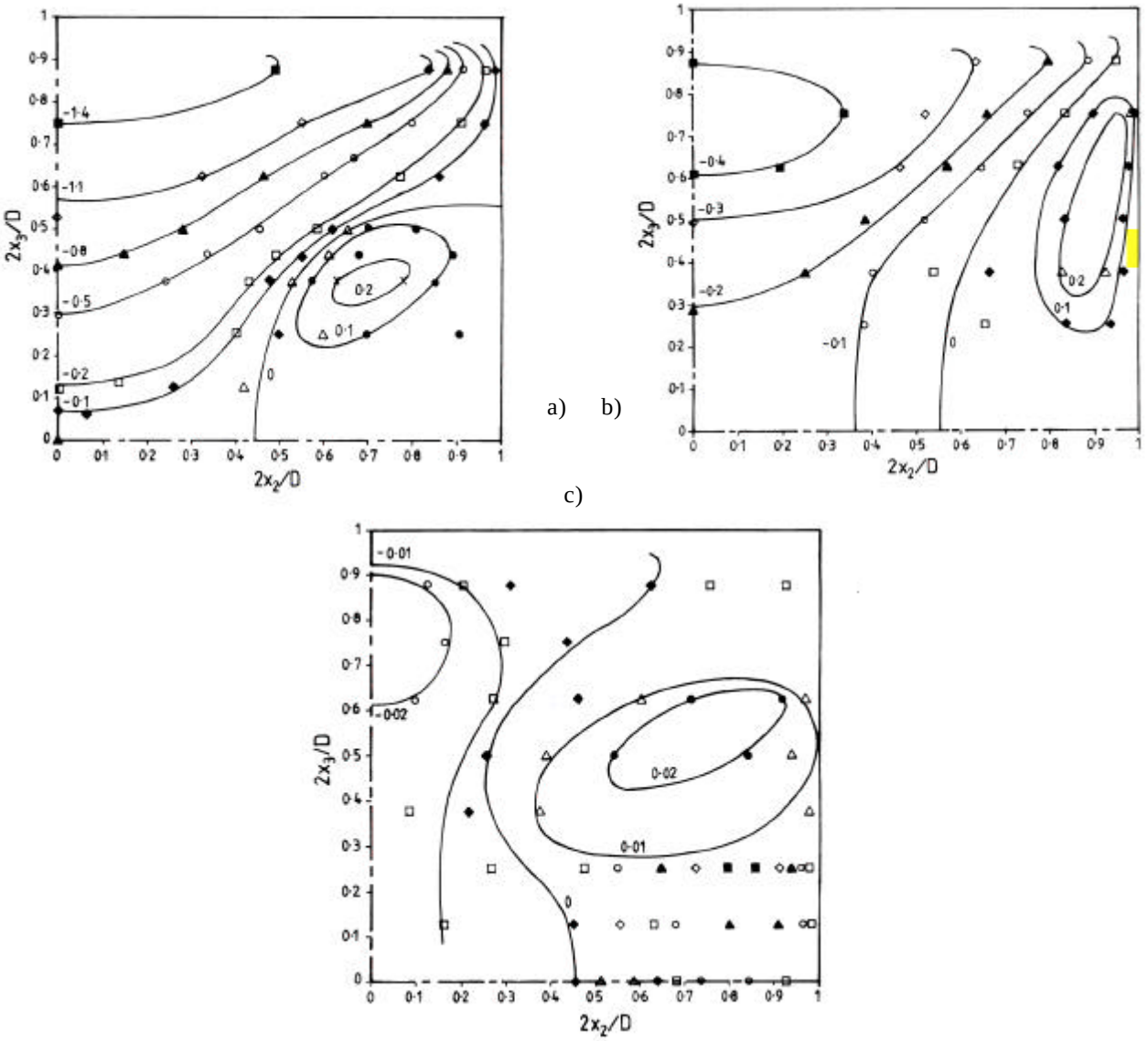

Figure 9. Contours of Reynolds shear stress $\overline{u_1 u_3}/U_C^2$ (a) water (b) CMC/XG (c) PAA.

6. Conclusions

The measurements reported here reveal a consistent picture of the combined effects of viscoelasticity and shear thinning on both the mean flow and turbulence structure of a non-Newtonian liquid flowing through a square duct. The reduction in the intensity of turbulent-velocity fluctuations transverse to the mean flow for CMC/XG is responsible for a reduction of nearly 80% in the secondary-flow velocities although the qualitative structure of both the primary axial flow and the secondary flow appears to be much the same as for a Newtonian fluid. As found in previous investigations of pipe and channel flow, the changes in the axial-velocity fluctuations are quite different from those in the transverse fluctuations, with the peak level increased and shifted away from the duct wall in the former case. For the transverse fluctuations the level is reduced and the peak location shifted away from the wall in actual distance but not to any significant extent in wall units.

For PAA, which is much more elastic than CMC/XG and leads to higher levels of drag reduction, the transverse-velocity fluctuations were suppressed to even lower levels than for CMC/XG. The axial-velocity fluctuations for PAA were also much reduced in intensity and found to be distributed much more axisymmetrically over the duct cross section than for the other two fluids with the peak moved even further from the duct wall in actual distance but by the same amount in wall units. Here too the transverse turbulence intensities are consistent with most previous investigations of pipe and channel flow. The corresponding Reynolds shear stress and the secondary-flow velocities were reduced to practically negligible levels and the primary axial flow for $\overline{u}_1/U_c \geq 0.4$ found to be distributed almost axisymmetrically with respect to the duct axis.

References

H A Barnes, J F Hutton, K Walters, An introduction to rheology, Elsevier (1989).

Y I Cho, J P Hartnett, Non-Newtonian fluids in circular pipe flow, Adv Heat Transfer15 (1982) 59.

A O Demuren, W Rodi, Calculation of turbulence-driven secondary motion in non-circular ducts, J Fluid Mech 140 (1984) 189.

M P Escudier, F Presti, S Smith, Drag reduction in the turbulent pipe flow of polymers, J Non-Newt Fluid Mech 81 (1999) 197.

B Gampert, A Rensch, Polymer concentration and near-wall turbulence structure of channel flow of polymer solutions, ASME FED-237, 1996 Fluids Eng Div Conf, 2 (1996) 129-136.

J P Hartnett, M Kostic, Turbulent friction factor correlations for power law fluids in circular and non-circular channels, Int Comm heat Mass Transfer, 17 (1990) 59.

J P Hartnett, E Y Kwack, B K Rao, Hydrodynamic behaviour of non-Newtonian fluids in a square duct, J Rheology 30 (S) (1986) S45.

J P Hartnett, B K Rao. Heat transfer and pressure drop for purely viscous non-Newtonian fluids in turbulent flow through rectangular passages, Wärme Stoffübertrag. 21 (1987) 261.

M Kostic, On turbulent drag and heat transfer reduction phenomena and laminar heat transfer enhancement in non-circular duct flow of certain non-Newtonian fluids, Int J Heat Mass Transfer 37, Suppl 1 (1994) 133.

M Kostic, J P Hartnett, Heat transfer performance of aqueous polyacrylamide solutions in turbulent flow through a rectangular channel, Int Comm Heat Mass Transfer. 12 (1985) 483.

W Kozicki, C H Chou, C Tiu, Non-Newtonian flow in ducts of arbitrary cross-sectional shape, Chem Eng Sci 21 (1966) 665.

W Kozicki, C Tiu, Improved parametric characterization of flow geometries, Can J Chem Eng 49 (1971) 562.

S E Logan, Laser velocity measurements of Reynolds stress and turbulence in dilute polymer solutions, AIAA J 10 (1972) 962-964.

A Melling, J H Whitelaw, Turbulent flow in a rectangular duct, J Fluid Mech 78 (1976) 289.

J Nikuradse, Turbulente Strömung in nichtkreisförmigen Rohren, Ing.-Arch. 1 (1930) 306.

J T Park, R J Mannheimer, T A Grimley, T B Morrow, Pipe flow measurements of a transparent non-Newtonian slurry, J Fluids Eng, 111 (1989) 331.

L Prandtl, The essentials of fluid dynamics, Blackie & Son Ltd, (1952).

F Presti, Private communication (1998).

M J Rudd, Velocity measurements made with a laser Dopplermeter on the turbulent pipe flow of a dilute polymer solution, J Fluid Mech 51 (1972) 673-685.

F M Wang, Y T Chew, B C Khoo, K S Yeo, Computation of turbulent flow in a square duct: aspects of the secondary flow and its origin, Computers in Fluids 23 (1994) 157.

M D Warholic, H Massah, T J Hanratty, Influence of drag-reducing polymers on turbulence: effects of Reynolds number, concentration and mixing, Expts. in Fluids 27 (1999) 461.

J A Wheeler, E H Wissler, Steady flow of non-Newtonian fluids in a square duct, Trans Soc Rheol 10 (1966) 353.